International Journal of Mathematics and Engineering Research
https://www.watchpub/ijmer/index.htm

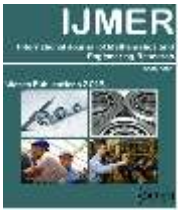

Numerical Simulations of Flow and Contaminant Transport Using Multiple Depth-Integrated Two-Equation Turbulence Models in the Yangtze River near the Nanjing City

Li-ren Yu[1,2].

[1]ESDV (Environmental Software and Digital Visualization), Rm.302, Unit4, Building420, Wan-Sheng-Bei-Li, Ton-Zhou Dist., 101121, Beijing, China.
[2]ASSER-CESUSC (Association of United Schools-Higher Education Center at São Carlos), Brazil.

Article Info:

Author(s):
Li-ren Yu.

History:
Received: 15-05-2013
Accepted Date: 1-06-2013

Vol 1 (1), pp, 001-013 June ,2013

Corresponding Author:
Li-ren Yu.
ASSER-CESUSC (Association of United Schools-Higher Education Center at São Carlos), Brazil.

E-mail: lirenyu@yahoo.com

Article Type:
Full Length Research

Keywords:
depth-integrated turbulence models; contaminant transport; numerical modeling; river modeling; multi-grid iterative method

Abstract

This paper reports a quasi 3D numerical simulation in a reach of the Yangtze River near The Nanjing City, China, aiming to develop a numerical tool for modeling turbulent flows and pollutant transport in natural waters. The recently built depth-integrated two-equation turbulence $\tilde{k}-\tilde{\omega}$ *model, together with* $\tilde{k}-\tilde{\varepsilon}$ and $\tilde{k}-\tilde{w}$ *models, were used to close non-simplified quasi 3D hydrodynamic fundamental governing equations. The discretized equations were solved by advanced multi-grid iterative method under non-orthogonal body-fitted coarse and fine two-levels' grids with collocated variable arrangement. Except for steady flow and transport computation, the processes of contaminant inpouring and plume development, caused by the side-discharge from two tributaries, also have been investigated numerically. The used three closure approaches are suitable for modeling strong mixing turbulence. The established* $\tilde{k}-\tilde{\omega}$ *model with higher order of magnitude of transported variable provides a possibility to elevate the computational precision. Based on the developed hydrodynamic model, a CFD (Computational Fluid Dynamics) software, namely Q3drm1.0, was developed. This tool focuses on the refined simulations of the steady and unsteady problems of flow and temperature/contaminant transports in complicated computational domains with the strong ability to deal with different types of discharges: side-discharge, point-source discharge/point-sink, and area-source discharge from the slope along bank. In this paper, only the study of side-discharge is presented.*

Introduction

Almost all flows in natural rivers are turbulence. Dealing with the problems of turbulence tightly related to stream pollutions is challenging for scientists and engineers, because of their damaging effect on our fragile environment and limited water resources. It is important to develop adequate mathematical models, turbulence closure models, numerical methods and corresponding analytical tools for timely simulating and predicting contaminant transport behaviors in natural and artificial waters.

Although the significance of modeling turbulent flows and contaminant transport phenomena with a high precision is clear, the numerical simulation and prediction for natural waters with complex geometry and variable bottom topography are still unsatisfied. This is mainly due to the inherent complexity of the problems being considered. Any computation and simulation of flow and transport processes critically depends on following four elements: to generate a suitable computational domain with the ability to deal with non-regular geometrical boundaries, such as curved riversides and island boundaries; to establish practical turbulence closure models with higher precision and minor numerical error; to adopt efficient computational method and algorithm, and to develop corresponding numerical tool, respectively.

Numerous environmental flows can be considered as shallow, *i.e.*, the horizontal length scales of the flow domain are much larger than the depth. Typical examples are found in lowland rivers, lakes, coastal areas, oceanic and stratified atmospheric flows. Depth-integrated mathematical models are frequently used for modelling the flow and contaminant transport in well-mixed shallow waters. However, many models used in practice merely consider the depth-integrated turbulent viscosity and diffusivity through constants or through simple phenomenological algebraic formulas (Choi and Takashi 2000; Lunis et al. 2004; Vasquez 2005; Kwan 2009; Viparelli 2010), which are estimated to a great degree according to the modeller's experience. Although some practical quasi 3D hydrodynamic models are really closed by depth-integrated two-equation closure turbulence model, they almost all concentrate on the investigations and applications of traditional depth-

integrated $\tilde{k}-\tilde{\varepsilon}$ model (Rodi et al. 1980; Chapman and Kuo 1982; Mei et al. 2002; Johnson et al. 2005; Cea et al. 2007; Hua et al. 2008; Kimura et al. 2009; Lee et al. 2011), which appeared already beyond 30 years. It is well known that the order of magnitude of transported variable $\tilde{\varepsilon}$ of $\tilde{k}-\tilde{\varepsilon}$ model is very low indeed.

Recent development of turbulence modeling theory has provided more advanced and realistic closure models. From an engineering perspective, two-equation closure turbulence models can build a higher standard for numerically approximation of main flow behaviors and transport phenomena in terms of efficiency, extensibility and robustness (Yu, 2013). Unfortunately, the 'standard' two-equation closure models, used widely in industry, cannot be directly employed in quasi 3D modeling. The depth-integrated turbulence model, based on the 'standard' two-equation closure model, needs to be established and investigated in advance.

Except for the depth-integrated $\tilde{k}-\tilde{\omega}$ model closure, newly established by the author, current simulations still adopt the closure approaches of traditional depth-integrated $\tilde{k}-\tilde{\varepsilon}$ model and depth-integrated $\tilde{k}-\tilde{w}$ model, respectively. The depth-integrated $\tilde{k}-\tilde{\omega}$ model was stemmed from the most common 'standard' *k-ω* model, originally introduced by Saffman (1970) but popularized by Wilcox (1998). In this paper, the results, computed by the three depth-integrated two-equation turbulence models, were compared each other. Such example, however, hardly exists for the simulation of contaminant transport in natural waters. Modeling by using different two-equation closure approaches will certainly increase the credibility of computed results (Yu, 2013).

On the other hand, recent advancements in grid generation techniques, numerical methods and IT techniques have provided suitable approaches to generate non-orthogonal boundary-fitted coordinates with collocated grid arrangement, on which the non-simplified hydrodynamic fundamental governing equations can be solved by multi-grid iterative method (Ferziger and Peric 2002). This paper describes a quasi 3D hydrodynamic simulation of flow and contaminant transport in a river reach of the Yangtze River, with the aim to develop the *grid-generator*, *flow-solver* and GUI (*Graphical User Interface*). The developed software, named **Q3drm1.0**, provides three selectable depth-integrated two-equation closure turbulence models, and can refinedly solve quasi 3D flow and contaminant transport phenomena in complex natural and artificial waters.

Hydrodynamic Fundamental Governing Equations

The complete, non-simplified fundamental governing equations of quasi 3D computation, in terms of coordinate-free vector forms derived by using vertical Leibniz integration for a Control Volume (CV, an arbitrary quadrilateral with center point *P*), considering the variation of the bottom topography and water surface and neglecting minor terms in the depth-averaging procedure, can be written as follows:

$$\frac{\partial}{\partial t}\int_{\Omega}\rho h\bar{\phi}d\Omega+\int_{S}\rho h\bar{\phi}\vec{v}\bullet\vec{n}dS=\int_{S}\Gamma h\mathbf{grad}\bar{\phi}\bullet\vec{n}dS+\int_{\Omega}\bar{q}_{\phi}d\Omega \quad (1)$$

where Ω is the CV's volume; S is the face; $\vec{v}$ is the depth-integrated velocity vector; the superscript " – " indicates that the value is strictly depth-integrated; $\bar{\phi}$ is any depth-integrated conserved intensive property (for mass conservation, $\bar{\phi}=1$; for momentum conservation, $\bar{\phi}$ is the components in different directions of $\vec{v}$; for conservation of a scalar, $\bar{\phi}$ is the conserved property per unit mass); Γ is the diffusivity for the quantity $\bar{\phi}$; $\bar{q}_{\phi}$ denotes the source or sink of $\bar{\phi}$; and *h* and ρ are local water depth at *P* and density, respectively.

For the momentum conservation of Eq. (1), $\Gamma=\tilde{\mu}_{eff}$ (depth-integrated effective viscosity); for temperature or concentration transport, Γ = $\tilde{\Gamma}_{\phi,t}$ (temperature or concentration diffusivity), where the superscript "~" indicates the quantity characterizing depth-integrated turbulence. The source (sink) term $\bar{q}_{\phi}$ for momentum conservation may include surface wind shear stresses, bottom shear stresses, pressure terms and additional point sources (or point sinks).

Depth-Integrated Turbulence Closure Models

The depth-integrated effective viscosity $\tilde{\mu}_{eff}$ and diffusivity $\tilde{\Gamma}_{\phi,t}$, appeared in Eq. (1), are dependent on the molecular dynamic viscosity μ and depth-integrated eddy viscosity $\tilde{\mu}_t$: $\tilde{\mu}_{eff}=\mu+\tilde{\mu}_t$ and $\tilde{\Gamma}_{\phi,t}=\tilde{\mu}_t/\sigma_{\phi,t}$, where $\sigma_{\phi,t}$ is the turbulence Prandtl number for temperature diffusion or Schmidt number for concentration diffusion, and $\tilde{\mu}_t$ is a scalar property and normally determined by two extra transported variables.

Recently, the author established a new depth-integrated two-equation closure turbulence model, $\tilde{k}-\tilde{\omega}$, based on the 'standard' k-ω model (in which *ω* is the special dissipation rate), originally introduced by Saffman (1970) but popularized by Wilcox (1998). The 'standard' k-ω turbulence model has been used in engineering researches (Riasi et al. 2009; Kirkgoz et al. 2009). In depth-integrated $\tilde{k}-\tilde{\omega}$ model, the turbulent viscosity is expressed by:

$$\tilde{\mu}_t=\rho\tilde{k}/\tilde{\omega} \quad (2)$$

where $\tilde{k}$ and $\tilde{\omega}$ stand for the depth-integrated turbulent kinetic energy and special dissipation rate of turbulence kinetic energy in the depth-integrated sense. They are determined by solving two extra transport equations, *i.e.*, the $\tilde{k}$ -eq. and $\tilde{\omega}$ -eq, respectively. (Yu and Yu, 2009):

$$\frac{\partial(\rho h\tilde{k})}{\partial t}+div(\rho h\tilde{k}\vec{v})=div(h(\mu+\frac{\tilde{\mu}_t}{\sigma_k^*})\mathbf{grad}\tilde{k})+hP_k-\rho\beta^* h\tilde{k}\tilde{\omega}+\rho hP_{kv}+\bar{S}_k \quad (3)$$

$$\frac{\partial(\rho h\tilde{\omega})}{\partial t}+div(\rho h\tilde{\omega}\vec{v})=div(h(\mu+\frac{\tilde{\mu}_t}{\sigma_\omega^*})\mathbf{grad}\tilde{\omega})+\alpha h\frac{\tilde{\omega}}{\tilde{k}}P_k-\rho h\beta\tilde{\omega}^2+\rho hP_{\omega v}+\bar{S}_\omega \quad (4)$$

where $\bar{S}_k$ and $\bar{S}_\omega$ are the source-sink terms, $P_k=\tilde{\mu}_t\left[2\left(\frac{\partial\bar{u}}{\partial x}\right)^2+2\left(\frac{\partial\bar{v}}{\partial y}\right)+\left(\frac{\partial\bar{u}}{\partial y}+\frac{\partial\bar{v}}{\partial x}\right)^2\right]$ is the production of turbulent kinetic energy due to the interactions of turbulent stresses with horizontal mean velocity gradients. The values of empirical constants α, β, β^*, σ_k^*, and σ_ω^* in Eq. (3) through Eq. (4) are the same as in the 'standard' $k-\omega$ model: 5/9, 0.075, 0.9, 2, and 2. According to the dimensional analysis, the additional source terms P_{kv} in *k*-eq. (3) and $P_{\omega v}$ in ω-eq. (4) are mainly produced by the vertical velocity gradients near the bottom, and can be expressed as follows:

$$P_{kv}=C_k u_*^3/h,\ P_{\omega v}=C_\omega u_*^2/h^2 \quad (5)$$

while the local friction velocity u_* is equal to $\sqrt{C_f\left(\bar{u}^2+\bar{v}^2\right)}$, the empirical constant C_ω for open channel flow and rivers can be expressed as:

$$C_\omega=\beta/(C_\mu\times e^*\times C_f^{1/2}) \quad (6)$$

where C_f represents an empirical friction factor and e^* is the dimensionless diffusivity of the empirical formula for undisturbed channel/river flows $\tilde{\mu}_t=e^*U_*h$ with U_* being the global friction velocity.

Except for the newly developed $\tilde{k}-\tilde{\omega}$ turbulence model mentioned above, the author also uses depth-integrated $\tilde{k}-\tilde{\varepsilon}$ model and $\tilde{k}-\tilde{w}$ model, to close the fundamental governing equations in the current computations. The $\tilde{k}-\tilde{\varepsilon}$ model was suggested by McGuirk and Rodi as early as in 1977:

$$\frac{\partial(\rho h\tilde{k})}{\partial t}+div(\rho h\tilde{k}\vec{v})=div(h(\mu+\frac{\tilde{\mu}_t}{\sigma_k})\mathbf{grad}\tilde{k})+hP_k-\rho h\tilde{\varepsilon}+\rho hP_{kv}+\bar{S}_k \quad (7)$$

$$\frac{\partial(\rho h\tilde{\varepsilon})}{\partial t}+div(\rho h\tilde{\varepsilon}\vec{v})=div(h(\mu+\frac{\tilde{\mu}_t}{\sigma_\varepsilon})\mathbf{grad}\tilde{\varepsilon})+C_1hP_k\frac{\tilde{\varepsilon}}{\tilde{k}}-C_2\rho h\frac{\tilde{\varepsilon}^2}{\tilde{k}}+\rho hP_{\varepsilon v}+\bar{S}_\varepsilon \quad (8)$$

where $\bar{S}_k$ and $\bar{S}_\varepsilon$ are the source-sink terms, $\tilde{\mu}_t$ can be expressed as:

$$\tilde{\mu}_t=\rho C_\mu\tilde{k}^2/\tilde{\varepsilon} \quad (9)$$

where $\tilde{\varepsilon}$ stands for dissipation rate of $\tilde{k}$. The values of empirical constants C_μ, σ_k, σ_ε, C_1 and C_2 in Eqs. (7-9) are the same as the 'standard' *k-ε* model, *i.e*. equal to 0.09, 1.0, 1.3, 1.44 and 1.92, respectively. The additional source terms P_{kv} and $P_{\varepsilon v}$ in Eqs. (7) and (8) can be written by:

$$P_{kv}=C_k u_*^3/h,\ P_{\varepsilon v}=C_\varepsilon u_*^4/h^2 \quad (10)$$

where the empirical constants C_k and C_ε for open channel flow and rivers are:

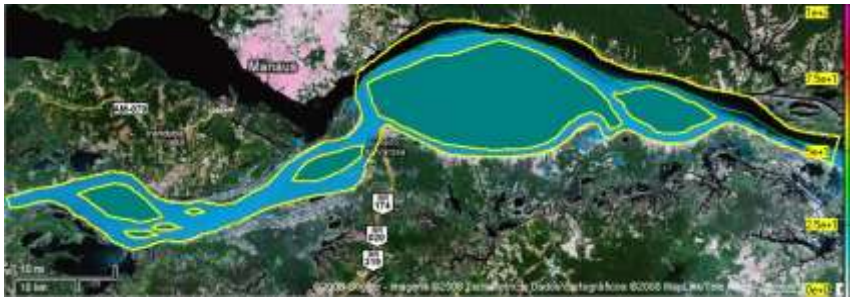

Figure 1: Comparison between calculated concentration contour and black-water plume outline.

$$C_k = 1/\sqrt{C_f}\ ,\ C_\varepsilon = C_2 C_\mu^{1/2}/(C_f^{3/4}\times e^{*1/2}) \qquad (11)$$

The third used depth-integrated second-order closure $\tilde{k}-\tilde{w}$ model was previously developed by the author of the present paper and his colleague (Yu and Zhang 1989). This model originated from the revised k-w model developed by Ilegbusi and Spalding (1982). The two extra transport equations of this model (*i.e.*, the $\tilde{k}$ -eq. and the $\tilde{w}$ -eq.) should be:

$$\frac{\partial(\rho h\tilde{k})}{\partial t} + div(\rho h\tilde{k}\vec{v}) = div(h(\mu + \frac{\tilde{\mu}_t}{\sigma_k})\mathbf{grad}\tilde{k}) + hP_k + \rho hP_{kv} - C_\mu \rho h\tilde{k}\tilde{w}^{1/2} + \bar{S}_k \qquad (12)$$

$$\frac{\partial(\rho h\tilde{w})}{\partial t} + div(\rho h\tilde{w}\vec{v}) = div(h(\mu + \frac{\tilde{\mu}_t}{\sigma_\varepsilon})\mathbf{grad}\tilde{w}) + C_{1w}\tilde{\mu}_t h(\mathbf{grad}\Omega)^2 \ - C_{2w}\rho h\tilde{w}^{3/2} f + C_{3w} h\frac{\tilde{w}}{\tilde{k}}P_k + \rho hP_{wv} + \bar{S}_w \qquad (13)$$

where $\bar{S}_k$ and $\bar{S}_w$ are the source-sink terms; function $f=1+C'_{2w}(\partial L/\partial x_i)$ and L is the characteristic distance of turbulence; Ω stands for mean movement vorticity. In $\tilde{k}-\tilde{w}$ model, the turbulent viscosity is defined as:

$$\tilde{\mu}_t = \rho\tilde{k}/\tilde{w}^{1/2} \qquad (14)$$

where $\tilde{w}$ is depth-integrated time-mean-square vorticity fluctuation of turbulence. The transport equations (the $\tilde{k}$ -eq. and $\tilde{w}$ -eq.) should be solved in this model as well. The values of empirical constants C_μ, σ_k, σ_w, C_{1w}, C_{2w}, C'_{2w} and C_{3w} are the same as those of 'standard' *k-w* model, *i.e.*, equal 0.09, 1.0, 1.0, 3.5, 0.17, 17.47 and 1.12, respectively. The corresponding additional source terms P_{kv} and P_{wv}, also mainly due to the vertical velocity gradients near the bottom, and can be expressed as:

$$P_{kv} = C_k u_*^3/h \qquad (15)$$

The empirical constants C_w for open channel flow and rivers can be written as:

$$C_w = C_{2w}/\left(C_\mu^{3/2}\times C_f^{3/4}\times e^{*3/2}\right) \qquad (16)$$

The mathematical model and turbulence models, developed by the author, have been numerically investigated with laboratorial and site data for different flow situations (Yu and Zhang 1989; Yu and Righetto 2001). In the established mathematical model, the original empirical constants of three depth-integrated turbulence models, suggested by their authors, are employed and have not been changed never.

Figure 1 displays a comparison between the fine light-blue concentration contour with 35*mg/L*, calculated by using $\tilde{k}-\tilde{\omega}$ model closure on fine grid and plotted by the field browser of **Q3drm1.0**, and the outline of black-water plume, shown on the *Google* satellite map. In this computation, one reach of the Amazon River, near the Manaus City, Brazil, has been computed, where the Negro River flows into the Solimões River from the North and the West to form the Amazon River below this city.

Figure 2: Map, plotted by *interface*.

Figure 3: Coarse grid.

The confluent tributaries, in the Amazon's water system, usually have concentration difference in comparison with the mainstream, caused by the humus in tropical rain forest (produced by tropic rains). The Negro River, however, is the largest left tributary of the Amazon and the largest black-water river in the world. In this figure, the coarse yellow lines demonstrate the outline of computational domain. It is clear that the simulated depth-integrated contour, however, is well coincident with the outline of black-water plume.

Grid Generation

In this paper, one reach of the Yangtze River has been computed by using the *grid-generator* and *flow-solver*, written in FORTRAN Language, where two small tributaries flow into the river reach from the left and right banks. The confluent tributaries have a concentration difference in comparison with the mainstream, caused by local industrial and domestic discharges. With the help of the developed software, it is possible to determine the scale of digital map (*Google Earth*), to collect conveniently geometrical data, including the positions of two riversides, four boundaries of two islands and the location of confluent tributaries' sections, and finally to generate one text file. In this file, all of messages, which illustrate necessary control variables and characteristic parameters, including those on four exterior boundaries (west and south inlet section, east and north outlet section, west and east riversides) are contained, and can be read by *grid-generator* to generate the expectant coarse and fine grids (two levels' grids).

Figure 2 demonstrates the digital map, on which the developed *interface* of **Q3drm1.0** has divided the computational river reach into 69 sub-reaches with 70 short cross-river lines (*i.e.*, NLrs=70). It is notable that the cross-river lines between the riverside and island boundary have been redrawn, in order to involve the islands' configurations. Figure 3 presents the generated body-fitted non-orthogonal coarse grid, drawn by the grid-browser of **Q3drm1.0**, with the resolution of 184 nodal points in *i*-direction and 20 nodal points in *j*-direction an, respectively. In the generated mesh, the nodal points on transversal grid lines are uniform. The total length of the calculated river reach is 26.172*km.* The flow direction is from the West and South to the East and North. The tributaries feed into the mainstream on the south riverside, with the numbers of nodal points from i=29 on the coarse computational grid, and on the north riverside, with the number of nodal points from i=104 to i=105, respectively. The two 'connected' islands start at (i=37, j=4) and (i=107, j=8), and ends at (i=116, j=4) and (i=128, j=8) on the same mesh, where 'connected' means NICVS(2)<NICVE(1), *i.e.* 107<116. It is clear that in this computational example, some cross-river lines have to connect with two islands. The developed *grid-generator* generated two layers' grids, on which all of geometric data, necessary in the later calculation of flow and contaminant transport, must be stored and then can be read by the developed *flow-solver*. The resolution of the fine grid is 366×38, displayed on Figure 4. This means that one volume cell on the coarse grid was divided into four volume cells on the fine grid. Figure 5 represents the bottom topography on fine grid, drawn by the field browser of **Q3drm1.0**. During the calculation, the variation of bottom topography was considered.

Solutions of Flow and Side Discharge

The behaviors of flows and transport were simulated by using the developed *flow-solver*, in which the SIMPLE (*Semi-Implicit Method for Pressure-Linked Equation*) algorithm for FVA (*Finite Volume Approach*), Guass'

Fig. 4 Fine grid.

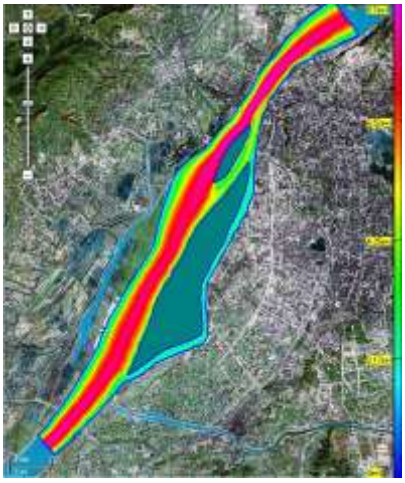

Fig. 5 Bottom topography.

divergence theorem, ILU (*Incomplete Lower-Upper*) decomposition, PWIM (*Pressure Weighting Interpolation Method*), SIP (*Strongly Implicit Procedure*), under relaxation and multi-grid iterative method have been used. The hydrodynamic fundamental governing equations were solved firstly at the coarse grid and then at the fine grid, in the following sequence for each grid level: two momentum equations ($\overline{u}$ -eq. and $\overline{v}$ -eq.), one pressure-correction equation (p' -eq.), one concentration transport equation ($\overline{C_1}$ -eq.), and two transport equations (*i.e.*, the $\tilde{k}$ -eq. and $\tilde{\varepsilon}$ -eq.; or $\tilde{k}$ -eq. and $\tilde{w}$ -eq.; or $\tilde{k}$ -eq. and $\tilde{\omega}$ -eq.), respectively.

The calculated main stream flow-rate is 20,000m^3/s, while the width, area and mean water-depth of the inlet section are 1211m, 7023m^2 e 5.8m. The empirical friction factor (C_f) equals 0.00175. The flow-rates and concentration differences of tributaries are 500m^3/s and 50mg/L, and 250m^3/s and 50mg/L, respectively. Three depth-integrated two-equation closure turbulence models, *i.e.,* the $\tilde{k}-\tilde{\varepsilon}$, $\tilde{k}-\tilde{w}$ and $\tilde{k}-\tilde{\omega}$ models, are adopted to close the quasi 3D hydrodynamic model. The turbulent variables at the inlet sections can be calculated by empirical formulae, *i.e.*, $\tilde{k}_0$, $\tilde{\varepsilon}_0$, $\tilde{w}_0$, $\tilde{\omega}_0$ are 0.179m^2/s^2, 0.00698m^2/s^3, 1.084/s^2, 0.432/s, and $\tilde{k}_{tri1}$ ($\tilde{k}_{tri2}$), $\tilde{\varepsilon}_{tri1}$ ($\tilde{\varepsilon}_{tri2}$), $\tilde{w}_{tri1}$ ($\tilde{w}_{tri2}$), $\tilde{\omega}_{tri1}$ ($\tilde{\omega}_{tri2}$) equal 0.025m^2/s^2(0.016m^2/s^2), 0.00107m^2/s^3(0.00042m^2/s^3), 0.449/s^2(0.1778/s^2), 0.474/s(0.298/s), respectively. On the outlet section, the variables satisfy constant gradient condition. The wall function approximation was used for determining the values of velocity components and turbulent variables at the nodal points in the vicinity of riversides and islands' boundaries.

Due to the existence of two islands in mesh, the values of the under-relaxation factors for velocity components, pressure, concentration and two turbulence parameters are usually lower than those while no exists any island in the mash. Generally, for non-existence of island, they are 0.6, 0.6, 0.1, 0.7, 0.7 and 0.7. In this example, these factors are 0.5, 0.5, 0.06, 0.7, 0.7 and 0.7, respectively. The maximum allowed numbers of inner iteration for solving velocity components, pressure, concentration and two turbulent variables are 1, 1, 20, 1, 1 and 1. The convergence criterions for inner iteration are 0.1, 0.1, 0.01, 0.1, 0.01 and 0.01, respectively. The α parameter of the Stone's solver is equal to 0.92. The normalize residuals for solving velocity field, pressure field, concentration field and the fields of two transported variables of turbulence are all less than pre-determined convergence criterion (1.e-3).

The simulation obtained various 2D and 3D distributions of flow, pressure, concentration and turbulent variables and parameters, which are useful to analyze interested problems in engineering. **Q3drm1.0** provides powerful profile browser, field browser and 3D browser for plotting and analyzing computational results. A part of results, simulated by using $\tilde{k}-\tilde{\varepsilon}$, $\tilde{k}-\tilde{w}$ and $\tilde{k}-\tilde{\omega}$ models on the fine grid, are presented from Figure 6 to Figure 12. Figure 6 display the results, calculated by using $\tilde{k}-\tilde{\omega}$ closure model and drawn by the field browser, with a: flow pattern, b: streamlines, c: pressure field, d: concentration contours, e: $\tilde{k}$ field and f: $\tilde{\omega}$ field, respectively. Figure 6d illustrates that two contaminant plumes well develop along both the right riverside and left riverside at the lower reaches of two tributaries' outlet sections. The distributions of the same depth-integrated physical variables and turbulent variable $\tilde{k}$, calculated by $\tilde{k}-\tilde{\varepsilon}$ and $\tilde{k}-\tilde{w}$ turbulence models, are similar to Figures 6a-6e. Figures 7a, 7b and 7c demonstrate the 3D distributions of $\tilde{k}$, calculated by using these three depth-integrated turbulence models

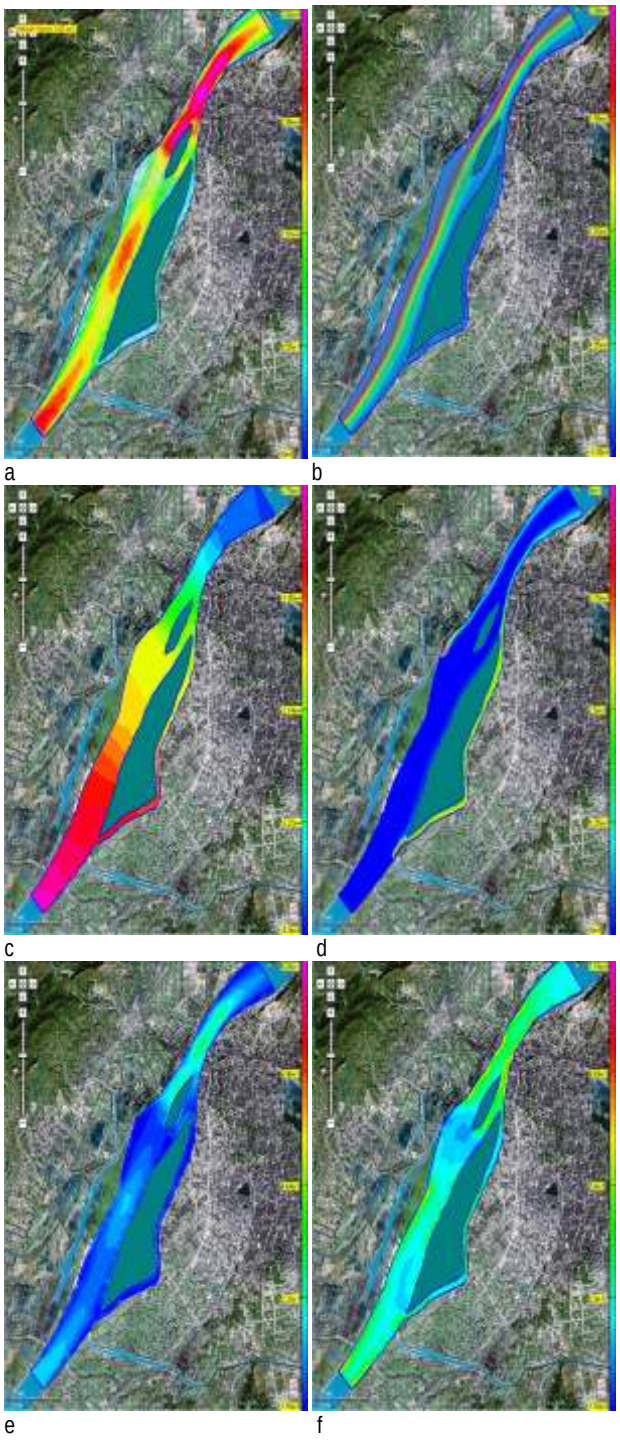

Fig. 6 A part of results, calculated by $\tilde{k}-\tilde{\omega}$ model.

and drawn by the 3D browser. They are quite similar each other, with the maximum values: 0.9259m^2/s^2 for $\tilde{k}-\tilde{\omega}$ modeling (7a), 0.9037m^2/s^2 for $\tilde{k}-\tilde{\varepsilon}$ modeling (7b) and 0.9021m^2/s^2 for $\tilde{k}-\tilde{w}$ modeling (7c), respectively. Figures 8a, 8b and 8c present the 3D distributions of $\tilde{\omega}$, $\tilde{\varepsilon}$ and $\tilde{w}$, which are different each other, because of the different definitions of the used second transported variables in current computations. Actually, the $\tilde{\varepsilon}$ value, shown in Figure 8b, ranges only from 1.012e-5 to 0.0335m^2/s^3; however, the $\tilde{w}$ and $\tilde{\omega}$ range from 1.065e-4 to 1.363/s^2 and from 1.034e-2 to 1.149/*s* in Figure 8c and Figure 8a respectively. Figures 9a, 9b and 9c illustrate the 3D distributions of effective viscosity $\tilde{\mu}_{eff}$, while the depth-integrated turbulent eddy viscosity $\tilde{\mu}_t$ was calculated by using Eq. (2) for $\tilde{k}-\tilde{\omega}$ modeling (9a), Eq. (9) for $\tilde{k}-\tilde{\varepsilon}$ modeling (9b) and Eq. (14) for $\tilde{k}-\tilde{w}$ modeling (9c), respectively. Basically, they are similar each other, specially for $\tilde{k}-\tilde{\varepsilon}$ and $\tilde{k}-\tilde{w}$ modeling, while the maximum values of $\tilde{\mu}_{eff}$ are 5115.43*Pa.s* (9b) and 5113.06*Pa.s* (9c); but the same value for $\tilde{k}-\tilde{\omega}$ modeling is 5175*Pa.s* (9a). Figure 10 shows the distributions of the production term of turbulent kinetic energy, with the maximum values of P_k 87.49*Pa.m/s* for $\tilde{k}-\tilde{\omega}$ modeling (10a), 87.093*Pa.m/s* for $\tilde{k}-\tilde{\varepsilon}$ modeling (10b) and 86.606*Pa.m/s* for $\tilde{k}-\tilde{w}$ modeling (10c). They are also similar each other. Figures 11a and 11b display the comparisons of concentration profiles along the centers of the volume cells at *i* from 1 to 366 and *j*=2 (*i.e.*, along a curved line from the outlet to the inlet near the east riverside) and at *i*=225 and *j* from 1 to 38 (*i.e.*, along a transversal section of *i*=225, which passes through two islands in computational domain), calculated by the depth-inegrated $\tilde{k}-\tilde{\varepsilon}$, $\tilde{k}-\tilde{w}$ and $\tilde{k}-\tilde{\omega}$ turbulence models, respectively. Figure 12a demonstrates the comparisons between $\tilde{\varepsilon}$, $\tilde{w}$ and $\tilde{\omega}$ along the curved line at *j*=3, and Figure 12b the comparisons of these three variables at *i*=225's transversal section. It is well known that the orders of magnitudes of $\tilde{\varepsilon}$, $\tilde{w}$ and $\tilde{\omega}$, used in three turbulence models, have significant differences indeed.

Contaminant Plume Development at the Beginning of Discharge

In order to well understand the development process of pollutant plume, a special simulation was performed by using $\tilde{k}-\tilde{\omega}$ model for the case described as follows. Supposing the contaminant concentrations of two confluent tributaries firstly to equal zero, and then, the value of concentration instantaneously reaches 50*mg/L* at *Time*=0, while the flow-rates, either of main stream or of tributaries, keep constant. Figures 13a-f illustrate the plumes' developments and variations in the lower reaches of two tributaries' outlet sections, where Figure 13a presents the situation of clean water confluence; Figures 13b-f display the process of contaminant

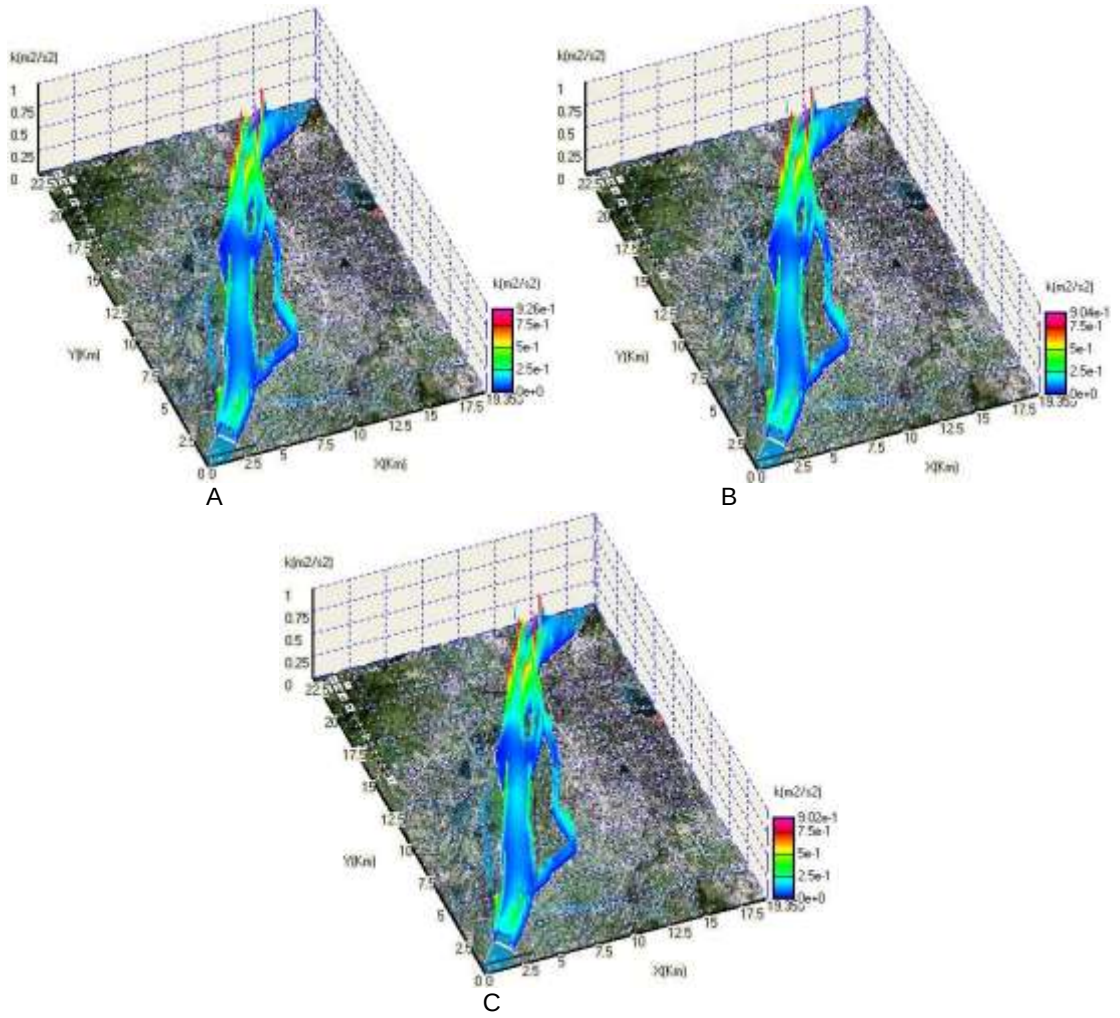

Figure 7: $\tilde{k}$ distributions, calculated by $\tilde{k}-\tilde{\omega}$, $\tilde{k}-\tilde{\varepsilon}$ and $\tilde{k}-\tilde{w}$ models.

inpouring and plumes' development, with an equal time difference *Δt* each other.

Discussions and Conclusions

Two-equation models are one of the most common types of turbulence closure models. The so-called 'standard' two-equation turbulence models, adopted widely in industry, cannot be directly used in depth-integrated modeling. Till now, the vast majority of quasi 3D numerical tools in the world, using two-equation turbulence model to solve complete and non-simplified hydrodynamic fundamental governing equations, just can provide only one depth-integrated turbulence model ($\tilde{k}-\tilde{\varepsilon}$) for users, which appears already beyond 30 years. However, the advanced commercial CFD (*Computational Fluid Dynamics*) software for 'standard' 2D and 3D modeling can provide several, even up to dozens of two-equation closure turbulence models, because there is non-existent a 'universal' turbulence closure model in turbulence modeling theory. Moreover, two-equation turbulence models are also very much still an active area of research and new refined two-equation models are still being developed. This situation should be changed as soon as possibly.

At present, the *k-ω* model, just like the *k-ε* model, has become industry standard model and is commonly used for most types of engineering problems. Therefore, the establishment of depth-integrated $\tilde{k}-\tilde{\omega}$ turbulence model and corresponding numerical investigation and comparison with existing depth-integrated turbulence models, presented in this paper, are significant.

Two levels' grids, one coarse mesh and one fine mesh, were used in current computation. The simulation on these two grids can satisfy the computational demand. If it is necessary, by setting the number of grid levels at three in the developed software, for example, the computations not only on coarse and fine grids but also on finest grid can be realized. The selection of the

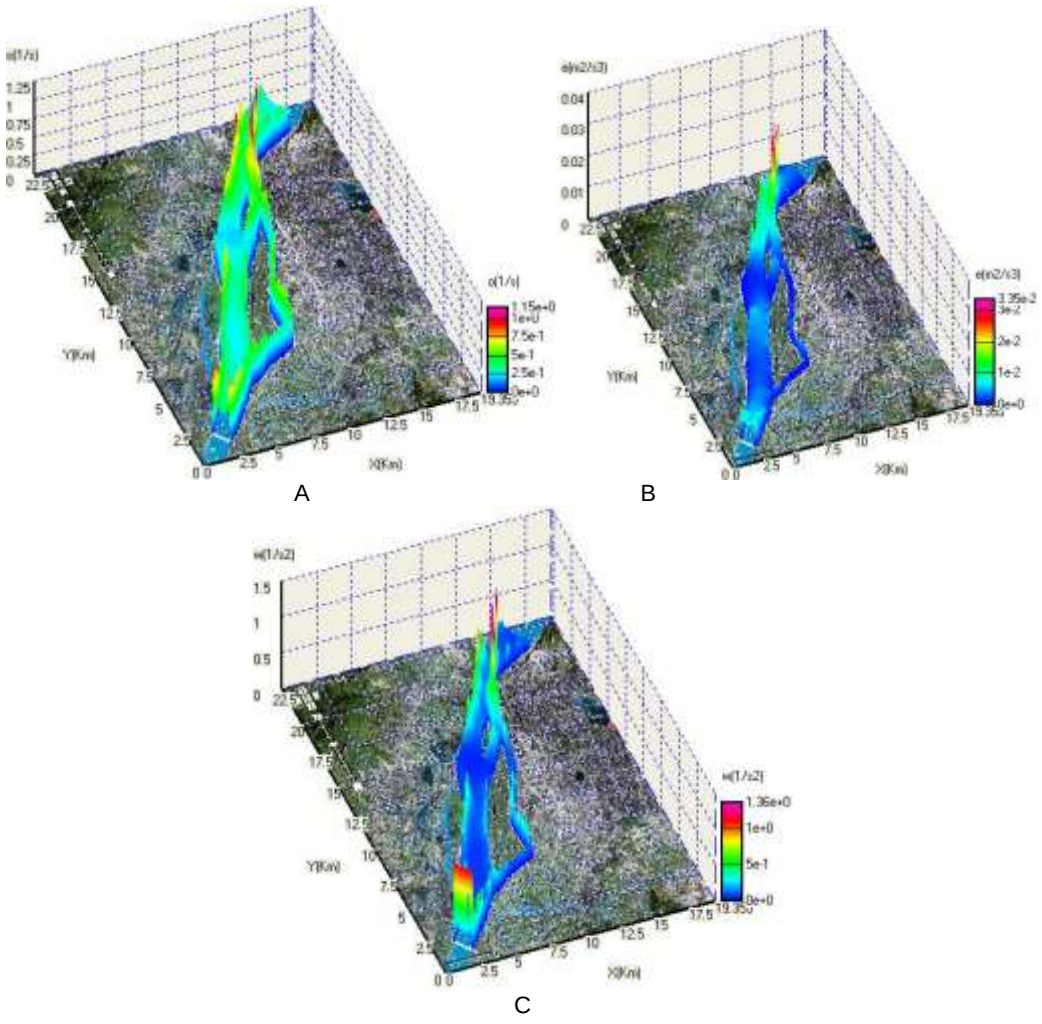

Figure 8: $\tilde{\omega}$, $\tilde{\varepsilon}$ and $\tilde{w}$ distributions.

number of grid levels depends on the solved problems, and also on modeler's requirements.

The solved depth-integrated concentration variable in current computation is the contaminant concentration difference between confluent tributaries and main stream (50*mg/L*). However, other indexes of discharged contaminant, such as COD and BOD, can be also considered as the solved variable. The developed software possesses the ability to simultaneously solve two concentration components in one calculation, which are produced by industrial and domestic discharges.

Figure 7 demonstrates that the distributions of turbulent variable $\tilde{k}$, calculated by three turbulence models, vary strongly in the computational domain, but quite similar to one another. However, the characteristics of the distributions of $\tilde{\omega}$, $\tilde{\varepsilon}$ and $\tilde{w}$, shown in Figures 8a, 8b and 8c, respectively, are quite different from one another, though they also vary sharply. The calculated effective viscosity $\tilde{\mu}_{eff}$, presented in Figures 9a, 9b and 9c, also varies strongly. In fact, the eddy viscosity changes from point to point in the computational domain, especially in the areas near the riversides and boundaries of islands. To solve the problems of contaminant transport caused by side discharge, for example, the plume usually develops along a region near riverside (see Figure 6d and Figure 13), where $\tilde{\mu}_t$ (or $\tilde{\mu}_{eff}$) actually varies much strongly (see Figure 9). This means that $\tilde{\mu}_t$ should be precisely calculated using suitable higher-order turbulence closure models with higher precision, and cannot be simply considered as an adjustable constant.

Figure 11 shows that the concentration profiles along the south riverbank, either calculated by $\tilde{k}-\tilde{\omega}$ and $\tilde{k}-\tilde{\varepsilon}$ closures, or calculated by $\tilde{k}-\tilde{w}$ closure, only have a quite small difference from one another. This means that three utilized depth-integrated two-equation turbulence models almost have the same ability to simulate plume distributions along riverbank. This conclusion also coincides with the result of author's

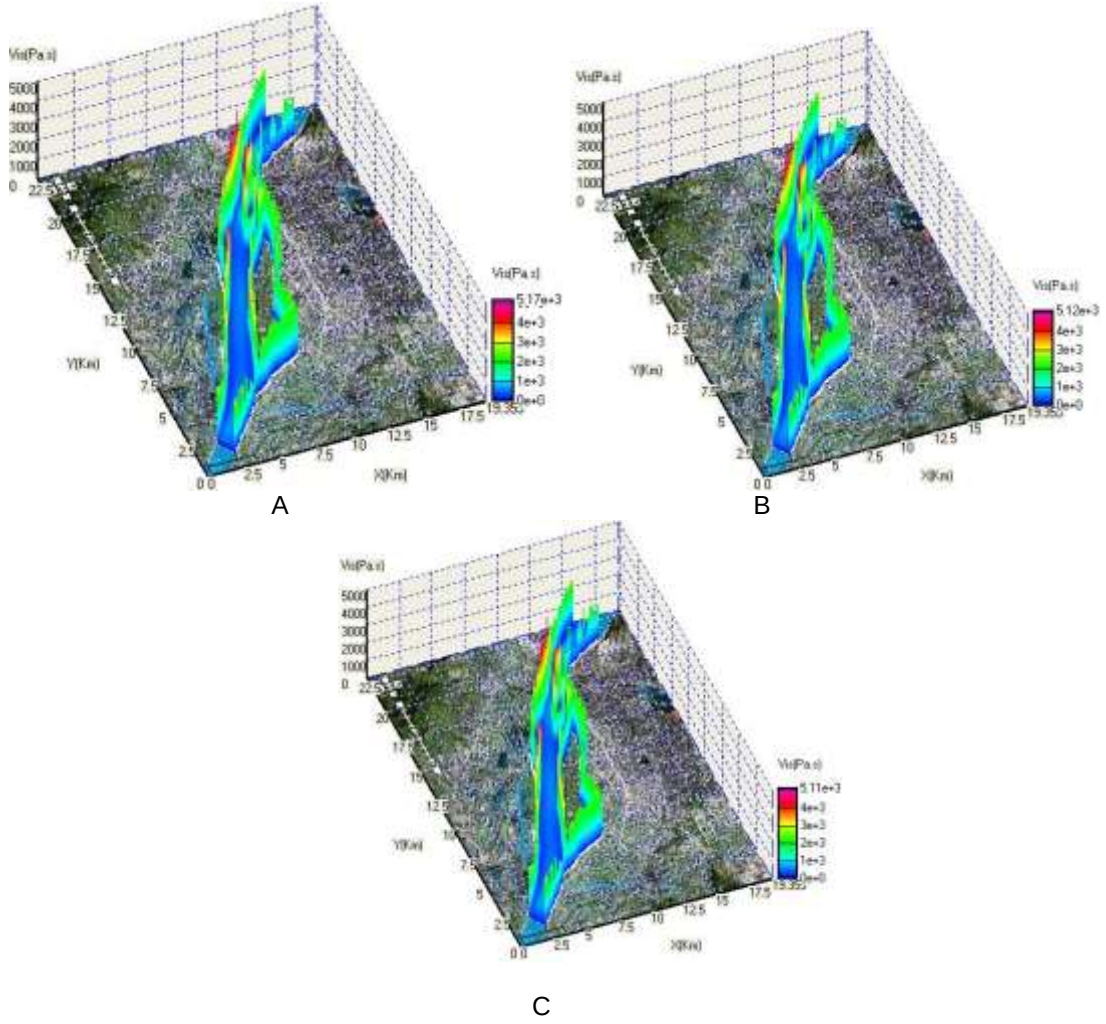

Figure 9: $\tilde{\mu}_{eff}$ distributions, calculated by $\tilde{k}-\tilde{\omega}$, $\tilde{k}-\tilde{\varepsilon}$ and $\tilde{k}-\tilde{w}$ models.

previous research that the depth-integrated two-equation turbulence models are suitable for modeling strong mixing turbulence (Yu and Righetto, 2001). However, the abilities and behaviors of different depth-integrated two-equation turbulence models for rather weak mixing, also often encountered in engineering, should be further investigated.

Except for the different definitions of transported variables: $\tilde{\varepsilon}$, $\tilde{w}$ and $\tilde{\omega}$, the order of magnitude of $\tilde{\varepsilon}$ is smaller than the order of magnitude of $\tilde{w}$, and much smaller than the order of magnitude of $\tilde{\omega}$. It should be noticed that three transported variables: $\tilde{\varepsilon}$, $\tilde{w}$ and $\tilde{\omega}$ all appear in the denominators of Eqs. (9), (14) and (2), which were used to calculate turbulent eddy viscosity $\tilde{\mu}_t$. For numerical simulation, the occurrence of numerical error is unavoidable, especially in the region near irregular boundary. It is clear that a small numerical error, caused by solving $\tilde{\varepsilon}$-eq., for example, will bring on larger error for calculating eddy viscosity than the same error caused by solving other two equations (*i.e.*, $\tilde{w}$-eq. and $\tilde{\omega}$-eq.). Without doubt, the elevation of the order of magnitude of used second turbulent variable, reflecting the advance of two-equation turbulence closure models, provides a possibility for users to improve their computational precision. The insufficiency of traditional depth-integrated $\tilde{k}-\tilde{\varepsilon}$ turbulence model may be avoided by adopting other turbulence models that have appeared recently, such as the $\tilde{k}-\tilde{\omega}$ model.

The developed *Graphical User Interface* of **Q3drm1.0** software can be used in various Windows-based microcomputers. The pre- and post-processors of this numerical tool, supported by a powerful self-contained map support tool together with a detailed help system, can help the user to easily compute the flows and contaminant transport behaviors in natural waters, closed by using three different depth-integrated two-equation turbulence models, and to draw and analyze various 2D and 3D engineering graphics for computed

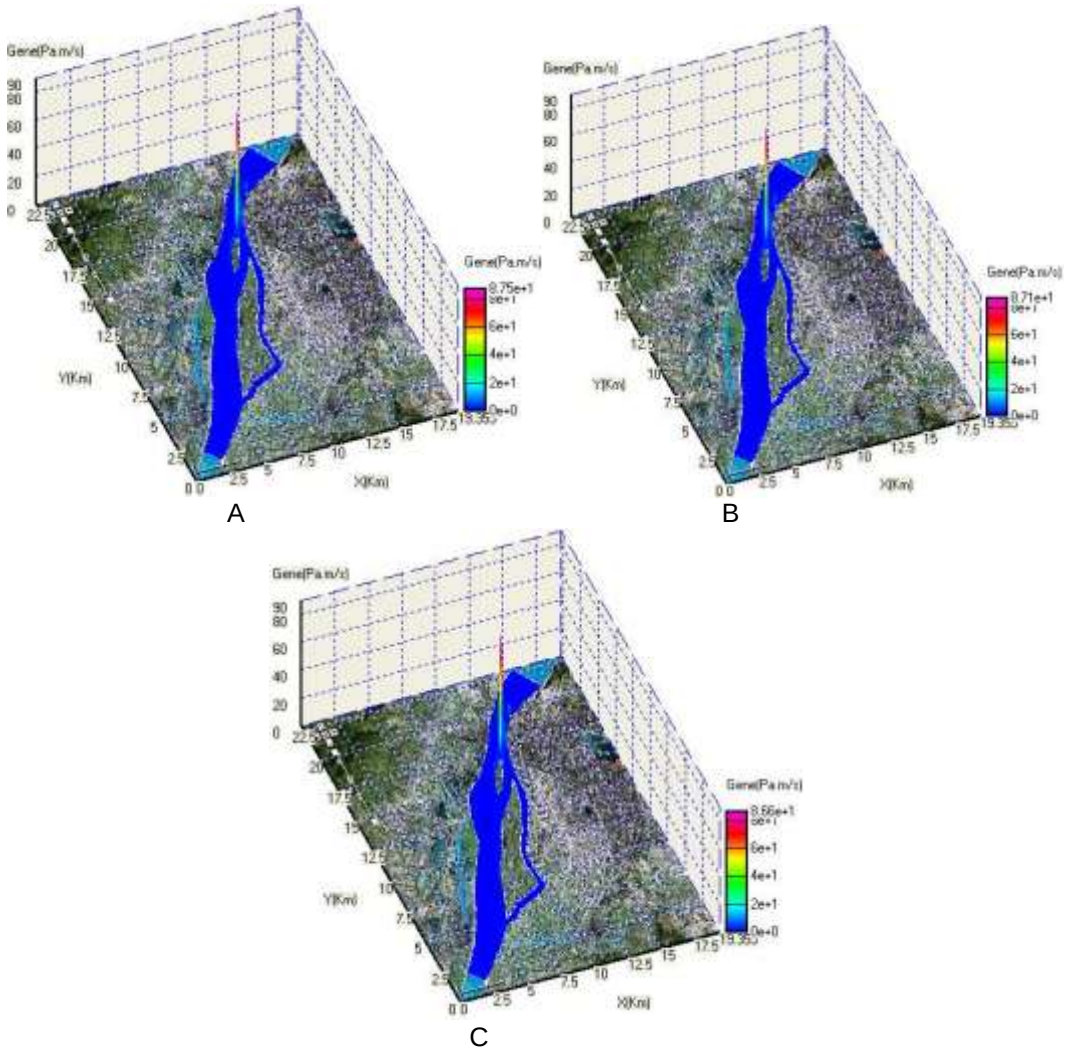

Figure 10: P_k distributions, calculated by $\tilde{k}-\tilde{\omega}$, $\tilde{k}-\tilde{\varepsilon}$ and $\tilde{k}-\tilde{w}$ models

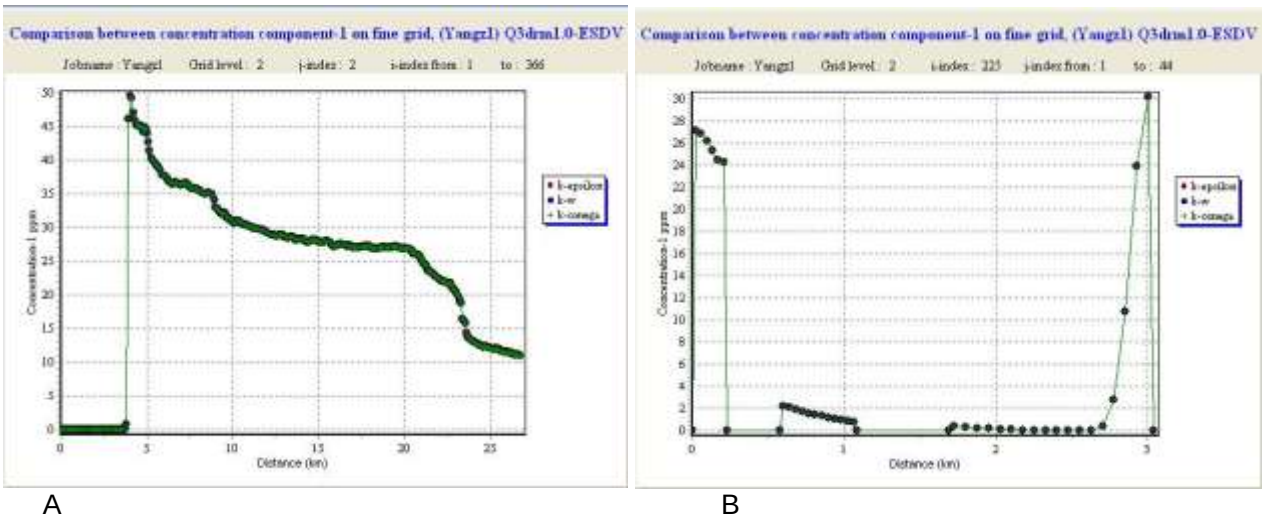

Figure 11: Concentrations at a: *i* from 1 to 366 and *j*=2; b: *i*=225 and *j* from 1 to 38.

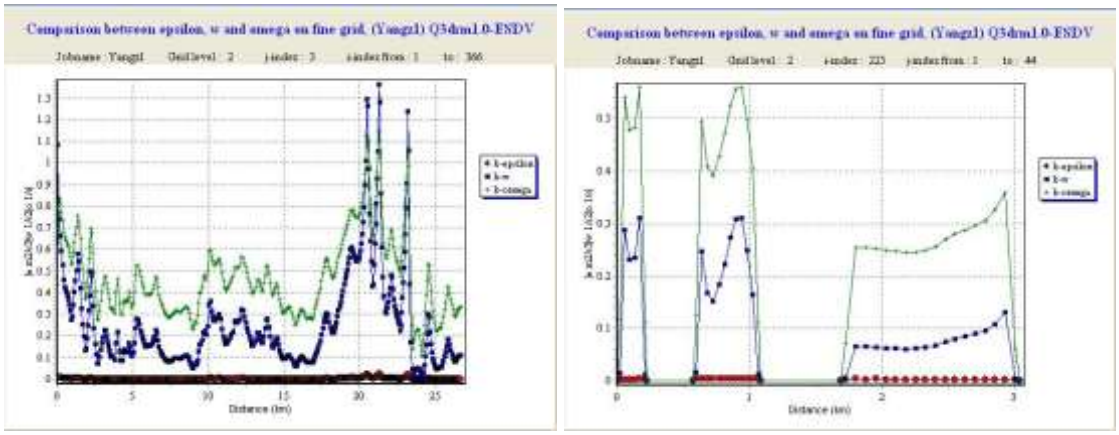

A B

Figure 12: $\tilde{\omega}$, $\tilde{\varepsilon}$ and $\tilde{w}$ at a: *i* from 1 to 366 and *j*=3; b: *i*=225 and *j* from 1 to 38.

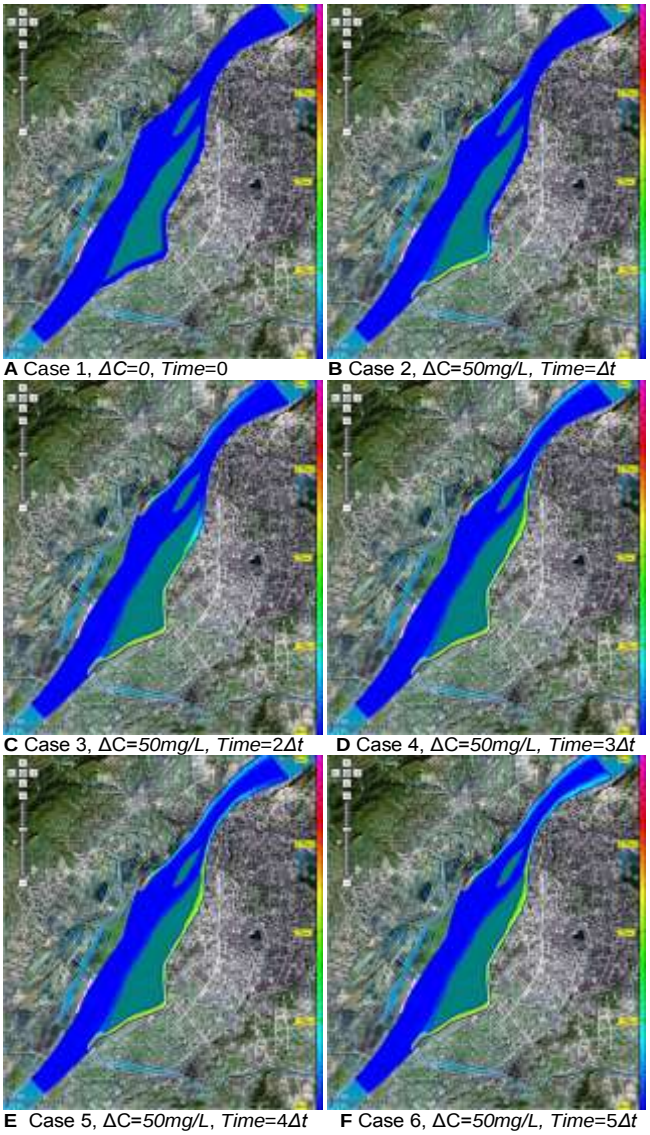

A Case 1, *ΔC=0*, *Time*=0 **B** Case 2, ΔC=*50mg/L*, *Time=Δt*

C Case 3, ΔC=*50mg/L*, *Time*=2*Δt* **D** Case 4, ΔC=*50mg/L*, *Time*=3*Δt*

E Case 5, ΔC=*50mg/L*, *Time*=4*Δt* **F** Case 6, ΔC=*50mg/L*, *Time*=5*Δt*

Figure 13: Contaminant plume development.

results (Yu, 2013).

Acknowledgement

The partial support of FAPESP through the Process No. PIPE 2006/56475-3 is gratefully acknowledged.

References

Cea L, Pena L, Puertas J, Vázquez-Cendón ME, Peña E (2007). Application of several depth-averaged turbulence models to simulate flow in vertical slot fishways. J. Hydraulic Engineering. 133(2): 160-172. http://dx.doi.org/doi/10.1061/(ASCE)0733-9429(2007)133:2(160)

Chapman RS, Kuo CY (1982). A Numerical Simulation of Two-Dimensional Separated Flow in a Symmetric Open-Channel Expansion Using the Depth-Integrated Two Equation (k-ε) Turbulence Closure Model. Dept. of Civ. Engrg., Rep. 8202, Virginia Polytechnic Inst. and State Univ., Blacksburg, VA.

Choi M, Takashi H (2000). A numerical simulation of lake currents and characteristics of salinity changes in the freshening process. J. Japan Society of Hydrol. Water Res., 13(6): 439-452. (in Japanese)

Ferziger JH, Peric M (2002). Computational Methods for Fluid Dynamics, 3rd Edition. Berlin, Springer.

Hua ZL, Xing LH, Gu L (2008). Application of a modified quick scheme to depth-averaged κ–ε turbulence model based on unstructured grids. J. Hydrodynamics Ser. B(4), 514-523. http://dx.doi.org/doi/10.1016 /S1001-6058(08)60088-8

Ilegbusi JO, Spalding DB (1982). Application of a New Version of the k-w Model of Turbulence to a Boundary Layer with Mass Transfer. CFD/82/15. London, Imperial College.

Johnson HK, Karambas TV, Avgeris I, Zanuttigh B,

Gonzalez-Marco D, Caceres I (2005). Modelling of waves and currents around submerged breakwaters. Coastal Engineering. 52(10): 949-969. http://dx.doi.org/doi/10.1016/j.coastaleng.2005.09.011

Kimura I, Uijttewaal WSJ, Hosoda T, Ali MS (2009). URANS computations of shallow grid turbulence. J. Hydraulic Engineering. 135(2): 118-131. http://dx.doi.org/doi/10.1061/(ASCE)0733-9429(2009)135:2(118)

Kirkgoz MS, Akoz MS, Oner AA (2009). Numerical modeling of flow over a chute spillway. J. Hydraulic Res., 47(6): 790-797.

Kwan S (2009). A Two Dimensional Hydrodynamic River Morphology and Gravel Transport Model. Master (MASc) Degree Thesis, Univ. British Columbia.

Lee JT, Chan HC, Huang CK, Wang YM, Huang WC (2011). A depth-averaged two-dimensional model for flow around permeable pile groins. International J. the Physical Sci., 6(6):1379-1387. http://dx.doi.org/doi/10.5897/IJPS11.078

Lunis M, Mamchuk VI, Movchan VT, Romanyuk LA, Shkvar EA (2004). Algebraic models of turbulent viscosity and heat transfer in analysis of near-wall turbulent flows. Inter. J. Fluid Mechanics Res., 31(3): 60-74. http://dx.doi.org/doi/10.1615/InterJFluidMechRes.v31.i3.60

McGuirk JJ, Rodi W (1977). A Depth-Averaged Mathematical Model for Side Discharges into Open Channel Flow. SFB 80/T/88. Universität Karlsruhe.

Mei Z, Roberts AJ, Li ZQ (2002). Modeling the Dynamics of Turbulent Floods. SIAM J. Applied Mathematics. 63(2): 423-458. http://dx.doi.org/doi/10.1137/S0036139999358866

Riasi A, Nourbakhsh A, Raisee M (2009). Unsteady turbulent pipe flow due to water hammer using *k*–ω turbulence model. J. of Hydraulic research. 47(4): 429-437. http://dx.doi.org/doi/10.1080/00221681003726247

Rodi W, Pavlovic RN, Srivatsa SK (1980). Prediction of flow pollutant spreading in rivers. In: Transport Models for Inland and Coastal Waters: Proceedings of the Symposium on Predictive Ability. Berkeley: University of California Academic Press, pp 63-111.

Saffman PG (1970). A model for inhomogeneous turbulent flow. In: Proc. Roy. Soc. London. A317, pp 417-433.

Vasquez JA (2005). Two Dimensional Finite Element River Morphology Model. Ph. D. Dissertation, University of British Columbia.

Viparelli E, Sequeiros OE, Cantelli A, Wilcock PR, Parker G (2010). River morphodynamics with creation/consumption of grain size stratigraphy 2: numerical model. Journal of Hydraulic Research. 48(6): 727-741. http://dx.doi.org/doi/doi:10.1080/00221686.2010.526759

Wilcox DC (1998). Turbulence Modeling for CFD. La Canada, DCW Industries, Inc.

Yu LR, Zhang SN (1989). A new depth-averaged two-equation ($\widetilde{k}-\widetilde{w}$) turbulent closure model. J. Hydrodynamics Series. B(1): 47-54.

Yu LR, Righetto AM (2001). Depth-averaged turbulence $\widetilde{k}-\widetilde{w}$ model and applications. Advances in Engineering Software. 32(5): 375-394. http://dx.doi.org/doi/10.1016/S0965-9978(00)00100-9

Yu LR, Yu J (2009). Numerical research on flow and thermal transport in cooling pool of electrical power station using three depth-averaged turbulence models. Water Science and Engineering. 2(3): 1-12. http://dx.doi.org/doi/10.3882/j.issn.1674-2370.2009.03.001

Yu LR (2013). Quasi 3D Modeling Flow and Contaminant Transport in Shallow Waters --- Using Multiple Depth-Averaged Two-Equation Closure Turbulence Models, CFD Software Development and Applications (ISBN: 978-3-659-33894-6). LAP LAMBERT Academic Publishing, Germany.